

Local Differential Privacy Image Generation Using Flow-based Deep Generative Models

Hisaichi Shibata^{a,*}, Shouhei Hanaoka^a, Yang Cao^b, Masatoshi Yoshikawa^c,
Tomomi Takenaga^a, Yukihiro Nomura^{d,e}, Naoto Hayashi^e, Osamu Abe^a

^a*Department of Radiology, The University of Tokyo Hospital, 7-3-1 Hongo, Bunkyo-ku,
Tokyo 113-8655, Japan*

^b*Graduate School of Information Science and Technology, Hokkaido University, Kita 14,
Nishi 9, Kita-ku, Sapporo, Hokkaido 060-0814, Japan*

^c*Department of Social Informatics Graduate School of Informatics, Kyoto University,
Yoshida-Honmachi, Sakyo-ku, Kyoto 606-8501, Japan*

^d*Center for Frontier Medical Engineering, Chiba University, 1-33 Yayoi-cho, Inage-ku,
Chiba 263-8522, Japan*

^e*Department of Computational Diagnostic Radiology and Preventive Medicine, The
University of Tokyo Hospital, 7-3-1 Hongo, Bunkyo-ku, Tokyo 113-8655, Japan*

Abstract

Diagnostic radiologists need artificial intelligence (AI) for medical imaging, but access to medical images required for training in AI has become increasingly restrictive. To release and use medical images, we need an algorithm that can simultaneously protect privacy and preserve pathologies in medical images. To develop such an algorithm, here, we propose DP-GLOW, a hybrid of a local differential privacy (LDP) algorithm and one of the flow-based deep generative models (GLOW). By applying a GLOW model, we disentangle the pixelwise correlation of images, which makes it difficult to protect privacy with straightforward LDP algorithms for images. Specifically, we map images onto the latent vector of the GLOW model, each element of which follows an independent normal distribution, and we apply the Laplace mechanism to the latent vector. Moreover, we applied DP-GLOW to chest X-ray images to generate LDP images while preserving pathologies.

Keywords: Differential Privacy, Deep Generative Models, Medical Images

*Corresponding author

Email address: sh@g.ecc.u-tokyo.ac.jp (Hisaichi Shibata)

¹This work was supported by JST, CREST Grant Number JPMJCR21M2, Japan

1. Introduction

Diagnostic radiologists need artificial intelligence (AI) for medical imaging to reduce workloads and enhance productivity. However, access to medical images required for the training of AI has become increasingly restrictive owing to the increasing demands for protection of personal information in each country. Moreover, data use agreements bind the purpose of use for even medical image datasets open to researchers upon request (e.g., [1]). Additionally, if someone specifies personal identities in medical images, irreversible leakage of personal information may occur.

Here, we assume a situation that we anonymize test datasets when training datasets are open to the public. We further assume that probabilistic distributions of medical images for the training and test datasets are similar. For example, the training dataset can be a large-scale dataset already open to the public from a hospital, and the test dataset can be a dataset privately held by another hospital.

Differential privacy (DP) algorithms [2] have recently emerged as tools with a weak privacy protection guarantee and usefulness. We specifically focus on local DP (LDP) [3], which adds noise to each image so that we cannot specify any identity in an image. Because one can anonymize the image upstream of image processing using LDP algorithms, we can use the processed images without limiting the purpose of use. At the same time, LDP can retain valuable information in the original image, e.g., lung opacity suggesting pneumonia in chest X-ray (CXR) images.

In previous studies [4, 5, 6, 7, 8, 9], LDP was not adopted for medical images. Therefore, previous studies did not evaluate the usefulness that LDP-processed images can contain valuable information for AI for medical imaging. In this study, we aim to evaluate the usefulness experimentally and quantitatively. As a metric of usefulness, we adopt the area under the curve (AUC) for pathology detection (we assume pneumonia detection in this study), which is essential in AI for medical imaging.

Because CXR images are the most representative medical images, in this study, we adopt CXR images from the Radiological Society of North America (RSNA) dataset. However, we can extend the proposed method to natural images and medical images of arbitrary modality and dimensions.

To summarize, our contributions are as follows:

1. We adopt a GLOW model [10] to disentangle image pixels and realize the ϵ -LDP algorithm for images (DP-GLOW).
2. We generate ϵ -LDP-processed CXR images.
3. We evaluate the usefulness of ϵ -LDP-processed CXR images using a pneumonia detection model.
4. We visually confirm how the proposed method obscures identities in medical images.

2. Related works

We briefly review previous studies on differential privacy algorithms for images implemented with deep models.

2.1. DP-SGD

Abadi et al. [11] proposed a differentially private stochastic gradient descent (DP-SGD) method, in which a controlled noise is added to the gradient of parameters and then clipped during the training of a deep model. Ziller et al. [12] proposed the training of a segmentation network for CXR images using a discriminative model trained with DP-SGD. Kossen et al. [13] proposed the generation of differentially private time-of-flight magnetic resonance angiography (TOF-MRA) images using generative adversarial networks (GANs) trained with DP-SGD. For DP-SGD, the theoretical guarantee that images generated using GANs trained with DP-SGD satisfy ϵ -LDP is not apparent.

2.2. LDP for images

Fan [8] adopted LDP (although it is not explicitly stated in the paper) for pixelized images. Image pixelization has the effect of reducing global sensitivity of the LDP algorithm. Fan [9] proposed another LDP algorithm using pixelization and Gaussian blur. Croft et al. [4], Liu et al. [7], and Li and Clifton [6] almost simultaneously proposed another LDP algorithm for images. Liu et al. [7] showed a concrete implementation using GANs, whereas Croft et al. [4] showed an abstract formulation. The implementation of the LDP algorithm for images by Li and Clifton is similar to that by Liu et al., but Li and Clifton adopt clipping so that the generated LDP images are within the probabilistic distribution of training images. Finally, Croft et al. [5] experimented with an LDP algorithm for facial obfuscation.

3. Preliminary for GLOW

Flow-based DGMs [14, 15, 10] learn an invertible map \mathbf{G}_θ^{-1} between a probabilistic distribution of images and a tractable probabilistic distribution (elementwise independent normal distribution in our settings). To this end, the flow-based DGMs maximize the average negative logarithm likelihood of training images during training. After the training, the flow-based DGMs can generate fake but realistic images (sampling) and can explicitly compute the value of the probabilistic density function of images (density estimation).

GLOW [10] is one of the flow-based DGMs. The deep network in GLOW recursively contains the actnorm, coupling, and permutation layers. The actnorm layer normalizes data. The coupling layer contains deep convolutional neural networks while it guarantees the invertibility of the layer. The permutation layer ensures that processing in coupling layers affects all the elements of data and is implemented using 1×1 convolution. Moreover, GLOW adopts a multiscale architecture, which can contain multiple deep networks of different recursive levels.

4. Our framework: DP-GLOW

We represent a gray-scale CXR image as a vector $\mathbf{x} \in \mathbf{R}^{H \times W}$, where H and W are the height and width of the image, respectively. We assume that the abovementioned GLOW has already been trained with many CXR images. Moreover, as a result of the training, we assume that we obtained an invertible map \mathbf{G}_θ^{-1} between an elementwise independent normal distribution and a probabilistic distribution of CXR images.

Our objective is to generate another image $\tilde{\mathbf{x}}$ from \mathbf{x} , which satisfies the definition of ϵ -LDP:

$$\log p(\tilde{\mathbf{x}}|\mathbf{x}) - \log p(\tilde{\mathbf{x}}|\mathbf{x}') \leq \epsilon, \quad (1)$$

where $\epsilon (> 0)$ is the privacy budget, \mathbf{x}' is an arbitrary image taken from a probabilistic distribution of CXR images, $p(\tilde{\mathbf{x}}|\mathbf{x})$ is the posterior probability to obtain $\tilde{\mathbf{x}}$ when we already obtained \mathbf{x} , and $p(\tilde{\mathbf{x}}|\mathbf{x}')$ is the posterior probability to obtain $\tilde{\mathbf{x}}$ when we already obtained \mathbf{x}' . To this end, we introduce a trained invertible vector function \mathbf{G}_θ^{-1} , which maps \mathbf{x} into another vector \mathbf{z} (a latent space vector), each element of which does not have a correlation with other elements. Such vector function is, in general, dependent on the

probabilistic distribution of images we adopt (e.g., CXR, head computed tomography, and mammography images). Therefore, we explicitly represent this dependence as parameters θ .

We define $\mathbf{z} \equiv \mathbf{G}_\theta^{-1}(\mathbf{x})$, $\mathbf{z}' \equiv \mathbf{G}_\theta^{-1}(\mathbf{x}')$, and $\tilde{\mathbf{z}} \equiv \mathbf{G}_\theta^{-1}(\tilde{\mathbf{x}})$. Because GLOW can ensure that each component of a latent space vector does not have a correlation if it is in the probabilistic distribution of training images for GLOW, we can straightforwardly apply the independent Laplace mechanism to the latent space by simply adding noise following the Laplace distribution:

$$\tilde{z}_k = z_k + \mathcal{N}_k, \quad (2)$$

$$\mathcal{N}_k \sim \text{Lap} \left(\mu_k = 0, \sigma_k = \frac{\Delta z_k}{\frac{\epsilon}{H \cdot W}} \right), \quad (3)$$

where μ_k and σ_k are respectively the expectation (a scalar) and scale (a scalar) of the Laplace distribution, ϵ is the user-defined privacy budget, and Δz_k is the sensitivity for the element k defined as

$$\Delta z_k := \max_{\mathbf{z}, \mathbf{z}': \mathbf{z} \neq \mathbf{z}'} |z_k - z'_k|, \quad (4)$$

where \mathbf{z} and \mathbf{z}' run latent vectors of all the training images. Moreover, we set a bound for each element of the latent space vector so that \mathbf{x} and $\tilde{\mathbf{x}}$ are in the probabilistic distribution of CXR images:

$$z_k \leftarrow \text{clip} \left(z_k, c_k - \frac{w_k}{2}, c + \frac{w_k}{2} \right), \quad (5)$$

$$\tilde{z}_k \leftarrow \text{clip} \left(\tilde{z}_k, c_k - \frac{w_k}{2}, c + \frac{w_k}{2} \right), \quad (6)$$

$$w_k = \alpha \cdot (\max_{\mathbf{z}} z_k - \min_{\mathbf{z}} z_k), \quad (7)$$

$$c_k = \frac{(\max_{\mathbf{z}} z_k + \min_{\mathbf{z}} z_k)}{2}, \quad (8)$$

where min and max operators respectively find the minimum and maximum values over all the latent space vectors \mathbf{z} for training images, the scalar function $\text{clip}(x, a, b)$ bounds the value of x such that $a \leq x \leq b$, and the subscript k means the element number (runs all the elements of the latent space vector). We set $\alpha = 0.4$ in this study. Now we can generate a differentially private image $\tilde{\mathbf{x}}$ for the budget ϵ ,

$$\tilde{\mathbf{x}} = \mathbf{G}_\theta(\tilde{\mathbf{z}}). \quad (9)$$

We prepare the vector function \mathbf{G}_θ^{-1} by training one of the flow-based DGMs, i.e., GLOW, with many CXR images prior to executing this locally differential private algorithm. We summarize our DP-GLOW algorithm to generate ϵ -LDP images below:

1. Train GLOW (maximize the average negative logarithm likelihood) with many CXR images to obtain \mathbf{G}_θ^{-1} .
2. Set the privacy budget ϵ .
3. Compute sensitivity from the training CXR images following Eq. (4).
4. Compute image-dependent clipping parameters following Eqs. (7) and (8) from the training CXR images.
5. Map an image \mathbf{x} from the test CXR images set onto the latent vector \mathbf{z} .
6. Clip \mathbf{z} following Eq. (5).
7. Add noise following Eq. (2) to obtain $\tilde{\mathbf{z}}$.
8. Clip $\tilde{\mathbf{z}}$ following Eq. (6).
9. Map the clipped latent vector $\tilde{\mathbf{z}}$ onto the CXR image space by \mathbf{G}_θ to obtain a ϵ -LDP CXR image.

Finally, we prove that our framework indeed satisfies ϵ -LDP. We can obtain the following equations using the change of variable formula:

$$\log p(\tilde{\mathbf{x}}|\mathbf{x}) = \log p(\tilde{\mathbf{x}}, \mathbf{x}) - \log p(\mathbf{x}) \quad (10)$$

$$\begin{aligned} &= \log p(\tilde{\mathbf{z}}, \mathbf{z}) + \log \left| \det \left(\frac{\partial(\tilde{\mathbf{z}}, \mathbf{z})}{\partial(\tilde{\mathbf{x}}, \mathbf{x})} \right) \right| \\ &- \log p(\mathbf{z}) - \log \left| \det \left(\frac{\partial \mathbf{z}}{\partial \mathbf{x}} \right) \right| \end{aligned} \quad (11)$$

$$= \log p(\tilde{\mathbf{z}}|\mathbf{z}) + \log \left| \det \frac{\partial \tilde{\mathbf{z}}}{\partial \tilde{\mathbf{x}}} \right| + \log \left| \det \frac{\partial \mathbf{z}}{\partial \mathbf{x}} \right| - \log \left| \det \frac{\partial \mathbf{z}}{\partial \mathbf{x}} \right| \quad (12)$$

$$= \log p(\tilde{\mathbf{z}}|\mathbf{z}) + \log \left| \det \frac{\partial \tilde{\mathbf{z}}}{\partial \tilde{\mathbf{x}}} \right|, \quad (13)$$

where we used the following modification:

$$\log \left| \det \left(\frac{\partial(\tilde{\mathbf{z}}, \mathbf{z})}{\partial(\tilde{\mathbf{x}}, \mathbf{x})} \right) \right| = \log \left| \begin{array}{cc} \frac{\partial \tilde{\mathbf{z}}}{\partial \tilde{\mathbf{x}}} & \frac{\partial \mathbf{z}}{\partial \tilde{\mathbf{x}}} \\ \frac{\partial \tilde{\mathbf{z}}}{\partial \mathbf{x}} & \frac{\partial \mathbf{z}}{\partial \mathbf{x}} \end{array} \right| \quad (14)$$

$$= \log \left| \begin{array}{cc} \frac{\partial \tilde{\mathbf{z}}}{\partial \tilde{\mathbf{x}}} & \frac{\partial \mathbf{z}}{\partial \tilde{\mathbf{x}}} \\ \mathbf{0} & \frac{\partial \mathbf{z}}{\partial \mathbf{x}} \end{array} \right| \quad (15)$$

$$= \log \left| \det \frac{\partial \tilde{\mathbf{z}}}{\partial \tilde{\mathbf{x}}} \right| + \log \left| \det \frac{\partial \mathbf{z}}{\partial \mathbf{x}} \right|. \quad (16)$$

We have $\frac{\partial \tilde{\mathbf{z}}}{\partial \mathbf{x}} = \mathbf{0}$ because vector \mathbf{z} is fixed and there is no correlation between probabilistic vector \mathcal{N} and any image vector \mathbf{x} .

Therefore, we have

$$\log p(\tilde{\mathbf{x}}|\mathbf{x}) = \log p(\tilde{\mathbf{z}}|\mathbf{z}) + \log \left| \det \frac{\partial \tilde{\mathbf{z}}}{\partial \tilde{\mathbf{x}}} \right|, \quad (17)$$

and

$$\log p(\tilde{\mathbf{x}}|\mathbf{x}') = \log p(\tilde{\mathbf{z}}|\mathbf{z}') + \log \left| \det \frac{\partial \tilde{\mathbf{z}}}{\partial \tilde{\mathbf{x}}} \right|. \quad (18)$$

Substituting those equations, we have

$$\log p(\tilde{\mathbf{x}}|\mathbf{x}) - \log p(\tilde{\mathbf{x}}|\mathbf{x}') = \log p(\tilde{\mathbf{z}}|\mathbf{z}) - \log p(\tilde{\mathbf{z}}|\mathbf{z}'). \quad (19)$$

Combined with the Laplace mechanism, we can ensure

$$\log p(\tilde{\mathbf{x}}|\mathbf{x}) - \log p(\tilde{\mathbf{x}}|\mathbf{x}') = \log p(\tilde{\mathbf{z}}|\mathbf{z}) - \log p(\tilde{\mathbf{z}}|\mathbf{z}') \quad (20)$$

$$= \sum_k^{H \cdot W} \log p(\tilde{z}_k|z_k) - \log p(\tilde{z}_k|z'_k) \quad (21)$$

$$= \sum_k^{H \cdot W} -\frac{|\tilde{z}_k - z_k|}{\frac{H \cdot W \cdot \Delta z_k}{\epsilon}} + \frac{|\tilde{z}_k - z'_k|}{\frac{H \cdot W \cdot \Delta z_k}{\epsilon}} \quad (22)$$

$$\leq \frac{\epsilon}{H \cdot W} \cdot \sum_k^{H \cdot W} \frac{|-z'_k + z_k|}{\Delta z_k} \quad (23)$$

$$\leq \epsilon, \quad (24)$$

where k runs each element of vectors.

5. Pneumonia detection with GLOW

Using the density estimation obtained by two trained flow-based DGMs and Bayes' theorem, Shibata et al. [16] proposed the computation of the logarithm posterior $\log p(C_n|\mathbf{x}_i)$, where C_n is a classification label that an image is a normal case, as follows:

$$\log p(C_n|\mathbf{x}_i) = \log p(\mathbf{x}_i|C_n) - \log p(\mathbf{x}_i) + \log p(C_n), \quad (25)$$

where $\log p(\mathbf{x}_i|C_n)$ is a conditional likelihood that we can estimate with a flow-based DGM trained with images of normal cases (\mathcal{M}_0), $\log p(\mathbf{x}_i)$ is a likelihood that we can estimate with the other flow-based DGM trained with images of normal and abnormal cases (\mathcal{M}_1), and $\log p(C_n)$ is a constant, which we can safely neglect when we draw the receiver operating characteristic curve (ROC curve) and thus when computing the area under the curve (AUC). We adopt the logarithm posterior to detect lung opacity suggesting pneumonia and other abnormalities from CXR images. We share \mathcal{M}_1 between DP-GLOW for generating ϵ -LDP CXR images and pneumonia detection with GLOW.

6. Numerical experiments

6.1. Dataset for CXR images

We took CXR images from the RSNA Pneumonia Detection Challenge dataset [17]. This dataset comprises 30,000 frontal-view CXR images, with each image labeled as “Normal,” “No Opacity/Not Normal,” or “Opacity” by one to three board-certified radiologists. The Opacity group consists of images with suspicious opacities suggesting pneumonia, and the No Opacity/Not Normal group consists of images with abnormalities other than pneumonia.

Table 1: Composition of datasets. $\mathcal{S}_{\text{normal}}^{\text{train}}$ and $\mathcal{S}_{\text{mixture}}^{\text{train}}$ share 6,529 normal CXR images.

Set	Normal	Abnormal
$\mathcal{S}_{\text{normal}}^{\text{train}}$	7,808	0
$\mathcal{S}_{\text{mixture}}^{\text{train}}$	6,553	6,631
$\mathcal{S}_{\text{unknown}}^{\text{test}}$	1,358	13,863

We show the composition of the CXR image sets in Table 1. We randomly sampled CXR images for the three datasets. We trained \mathcal{M}_0 with $\mathcal{S}_{\text{normal}}^{\text{train}}$ and we trained \mathcal{M}_1 with $\mathcal{S}_{\text{mixture}}^{\text{train}}$. In order not to strongly obfuscate lung opacity suggesting pneumonia, we created locally differential private CXR images using the DGM model \mathcal{M}_1 , i.e., we adopted \mathbf{G}_{θ}^{-1} of \mathcal{M}_1 for the DP-GLOW algorithm. We used images in $\mathcal{S}_{\text{unknown}}^{\text{test}}$ to create ϵ -LDP-CXR images with DP-GLOW and detect pneumonia from the ϵ -LDP-CXR images.

Table 2: Hyperparameters for GLOW.

Coupling layer	Affine
Learn-top option	False
Flow permutation	1×1 convolution
Minibatch size	4
Number of training samples per epoch	50,000
Network levels	7
Depth per level	32
Image size (in pixel)	$H512 \times W512 \times C1$
Total epochs	200
Learning rate in steady state	10^{-3}

6.2. Hyperparameters

We show the hyperparameters for the training of CXR image sets $\mathcal{S}_{\text{normal}}^{\text{train}}$ and $\mathcal{S}_{\text{mixture}}^{\text{train}}$ in Table 2. To train GLOW, we used Tensorflow 1.12.0. The versions of CUDA and cuDNN were 9.0.176 and 7.4, respectively. We carried out all processes in one computing node of the Reedbush-L supercomputer system in the Information Technology Center, The University of Tokyo. The system consists of 64 computing nodes equipped with two Intel Xeon E5-2695v4 processors, 256 GB memory, and four GPUs (NVIDIA Tesla P100 SXM2 with 16 GB memory).

To obtain ϵ -LDP-CXR images and to detect pneumonia in CXR images, we used Tensorflow 1.15.5. The versions of CUDA and cuDNN were 9.0 and 8.1, respectively. We carried out all processes in one computing node of the Wisteria/B-DEC01 supercomputer system in the Information Technology Center, The University of Tokyo. The system (Wisteria-Aquarius) consists of 45 computing nodes equipped with two Intel Xeon 8360Y processors and eight GPUs (NVIDIA A100 with 40 GB memory).

7. Results

7.1. ϵ -LDP-processed CXR images

In Fig. 1, we show four ϵ -LDP-processed CXR images of clinical cases obtained with the image domain LDP, which directly imposes the Laplace mechanism on the input image, with different privacy budgets together with

the original images. Fig. 2 shows four ϵ -LDP-processed CXR images of clinical cases obtained with DP-GLOW and different privacy budgets together with the original images. In case 1 for DP-GLOW, there is decreased permeability in the bilateral hilar regions. Although this hilar opacity tends to be preserved with a larger privacy budget, the entire image is degraded when the privacy budget becomes $10^1 \cdot H \cdot W$. A similar tendency is observed in the images of all the four cases for DP-GLOW; for example, in case 4 with $\epsilon = 10^1 \cdot H \cdot W$, the lung opacity suggesting pneumonia in the right lower lung field is well preserved, while the entire image is degraded.

7.2. Qualitative assessment of LDP-processed CXR images

Here, we assume two possible privacy leakage scenarios. To CXR images, we intentionally add features that can lead to the re-identification of the subject appearing in a CXR image. The first feature is an artificial block marker. The second feature is a rare anatomical abnormality known as *situs inversus* simulated by flipping a CXR image along the vertical axis. Figs. 3(a) and 3(c) show CXR images with the artificial block marker. Fig. 5(a) shows a flipped CXR image to represent a case of *situs inversus*. We applied DP-GLOW to these CXR images. In Figs. 3(b) and 3(d), the image domain LDP fails to obfuscate the artificial block marker with a moderate privacy budget. In contrast, in Figs. 4(b) and 4(d), DP-GLOW successfully obfuscated the artificial block marker with the moderate privacy budget. On the other hand, the anatomical shape of the chest and the abnormal opacity (hilar regions in the case 1) are preserved. In Fig. 5(b), we observed that the right edge of the heart does not become obfuscated with the image domain LDP. In contrast, in Fig. 6(b), we observed that the right edge of the heart becomes obfuscated and the heart appears at the center of the thoracic cage with DP-GLOW. However, DP-GLOW with this privacy budget is insufficient to almost completely erase the feature of *situs inversus*.

7.3. Pneumonia detection in ϵ -LDP-processed CXR images

Table 3 shows the area under the curve (AUC) with different privacy budgets for ϵ -LDP-processed CXR images obtained with the image domain LDP and DP-GLOW.

8. Discussion

We showed an algorithm (DP-GLOW) for generating useful images for diagnosis and medical AI, while ϵ -LDP is guaranteed against any image in

Table 3: AUC for pneumonia detection.

ϵ [-]	AUC (Image Domain LDP) [-]	AUC (DP-GLOW) [-]
∞ (without clip)	0.807	0.807
$10^3 \cdot H \cdot W$	0.813	0.679
$10^2 \cdot H \cdot W$	0.559	0.665
$10^1 \cdot H \cdot W$	0.643	0.539

the training distribution. Furthermore, this is the first study to apply an ϵ -LDP algorithm against a medical image itself. Additionally, we validated the usefulness of the ϵ -LDP CXR images generated by AI for pneumonia detection: we, for the first time, showed the AUC as a function of the privacy budget. Finally, this is the first work to adopt flow-based DGMs for LDP processing.

For DP-GLOW, the AUCs for pneumonia detection significantly change from 0.539 to 0.807, while the privacy budget varies from $10^1 \cdot H \cdot W (= 2,621,440)$ to ∞ . This means that this range of the privacy budget is indeed meaningful whereas the privacy budget is very large compared with usual values of ϵ -LDP for scalar quantities. This finding implies that we must normalize the privacy budget so that we can consistently handle ϵ -LDP for vector quantities. To normalize the budget, we compute the privacy budgets per image pixel. To this end, we intentionally indicated the privacy budget to have a common factor $H \cdot W$. Therefore, the actual privacy budgets per image pixel in this study are from 10^1 to ∞ , which are not much larger than commonly accepted privacy budgets.

Most of the approximate forms in CXR images are preserved and privacy is not protected with the image domain LDP. On the other hand, given a low privacy budget, DP-GLOW deforms the image so much that individuals cannot be identified. However, the AUCs for pneumonia detection are similar with the low privacy budget between DP-GLOW and the image domain LDP.

This study has several future directions. First, we adopted CXR images but one can adopt other kinds of image including nonmedical images. Second, we can easily extend this method to three-dimensional (3D) flow-based DGMs to generate ϵ -LDP 3D images. Third, we can use other flow-based DGMs different from GLOW.

This study has a limitation. We must train GLOW with many medical images to generate ϵ -LDP-processed medical images by DP-GLOW. The

training is very difficult when medical images of interest are not available. However, once the GLOW is trained with the medical images of interest, we can distribute the GLOW model to further release medical images of the same kind to the public using DP-GLOW.

9. Conclusion

We proposed DP-GLOW, the ϵ -LDP algorithm for images built upon the flow-based DGMs, which can simultaneously ensure privacy protection and preservation of pathologies with a controllable privacy budget. The ϵ -LDP-processed CXR images obtained with DP-GLOW indicate that we have obtained a powerful tool to release and use medical images for training AI.

References

- [1] Alzheimer’s disease neuroimaging initiative, <https://adni.loni.usc.edu/>, [Online; accessed 1 November 2022].
- [2] C. Dwork, Differential privacy: A survey of results, in: International conference on theory and applications of models of computation, Springer, 2008, pp. 1–19.
- [3] Ú. Erlingsson, V. Pihur, A. Korolova, Rappor: Randomized aggregatable privacy-preserving ordinal response, in: Proceedings of the 2014 ACM SIGSAC Conference on Computer and Communications Security, 2014, pp. 1054–1067.
- [4] W. L. Croft, J.-R. Sack, W. Shi, Obfuscation of images via differential privacy: From facial images to general images, *Peer-to-Peer Networking and Applications* 14 (3) (2021) 1705–1733.
- [5] W. L. Croft, J.-R. Sack, W. Shi, Differentially private facial obfuscation via generative adversarial networks, *Future Generation Computer Systems* 129 (2022) 358–379.
- [6] T. Li, C. Clifton, Differentially private imaging via latent space manipulation, arXiv preprint arXiv:2103.05472.
- [7] B. Liu, M. Ding, H. Xue, T. Zhu, D. Ye, L. Song, W. Zhou, DP-Image: Differential privacy for image data in feature space, arXiv preprint arXiv:2103.07073.

- [8] L. Fan, Image pixelization with differential privacy, in: IFIP Annual Conference on Data and Applications Security and Privacy, Springer, 2018, pp. 148–162.
- [9] L. Fan, Differential privacy for image publication, in: Theory and Practice of Differential Privacy (TPDP) Workshop, Vol. 1, 2019, p. 6.
- [10] D. P. Kingma, P. Dhariwal, Glow: Generative flow with invertible 1x1 convolutions, Advances in Neural Information Processing Systems 31.
- [11] M. Abadi, A. Chu, I. Goodfellow, H. B. McMahan, I. Mironov, K. Talwar, L. Zhang, Deep learning with differential privacy, in: Proceedings of the 2016 ACM SIGSAC conference on computer and communications security, 2016, pp. 308–318.
- [12] A. Ziller, D. Usynin, R. Braren, M. Makowski, D. Rueckert, G. Kaissis, Medical imaging deep learning with differential privacy, Scientific Reports 11 (1) (2021) 1–8.
- [13] T. Kossen, M. A. Hirzel, V. I. Madai, F. Boenisch, A. Hennemuth, K. Hildebrand, S. Pokutta, K. Sharma, A. Hilbert, J. Sobesky, I. Galinovic, A. Khalil A, J. Fiebach B, D. Frey, Toward sharing brain images: Differentially private tof-mra images with segmentation labels using generative adversarial networks, Frontiers in Artificial Intelligence 5.
- [14] L. Dinh, D. Krueger, Y. Bengio, Nice: Non-linear independent components estimation, arXiv preprint arXiv:1410.8516.
- [15] L. Dinh, J. Sohl-Dickstein, S. Bengio, Density estimation using real nvp, arXiv preprint arXiv:1605.08803.
- [16] H. Shibata, S. Hanaoka, Y. Nomura, T. Nakao, I. Sato, D. Sato, N. Hayashi, O. Abe, Versatile anomaly detection method for medical images with semi-supervised flow-based generative models, International Journal of Computer Assisted Radiology and Surgery 16 (12) (2021) 2261–2267.
- [17] G. Shih, C. C. Wu, S. S. Halabi, M. D. Kohli, L. M. Prevedello, T. S. Cook, A. Sharma, J. K. Amorosa, V. Arteaga, M. Galperin-Aizenberg, et al., Augmenting the national institutes of health chest radiograph dataset with expert annotations of possible pneumonia, Radiology: Artificial Intelligence 1 (1) (2019) e180041.

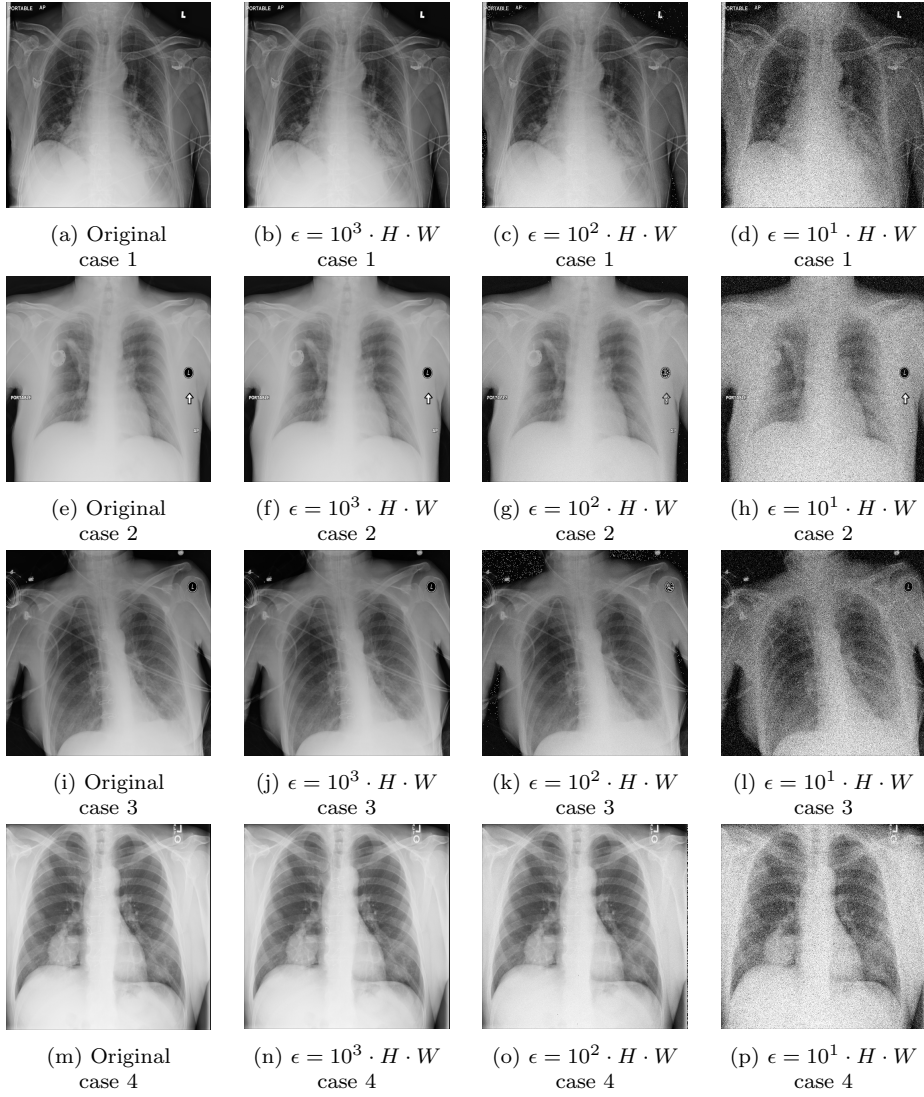


Figure 1: ϵ -LDP-processed CXR images (we applied the Laplace mechanism in the image domain).

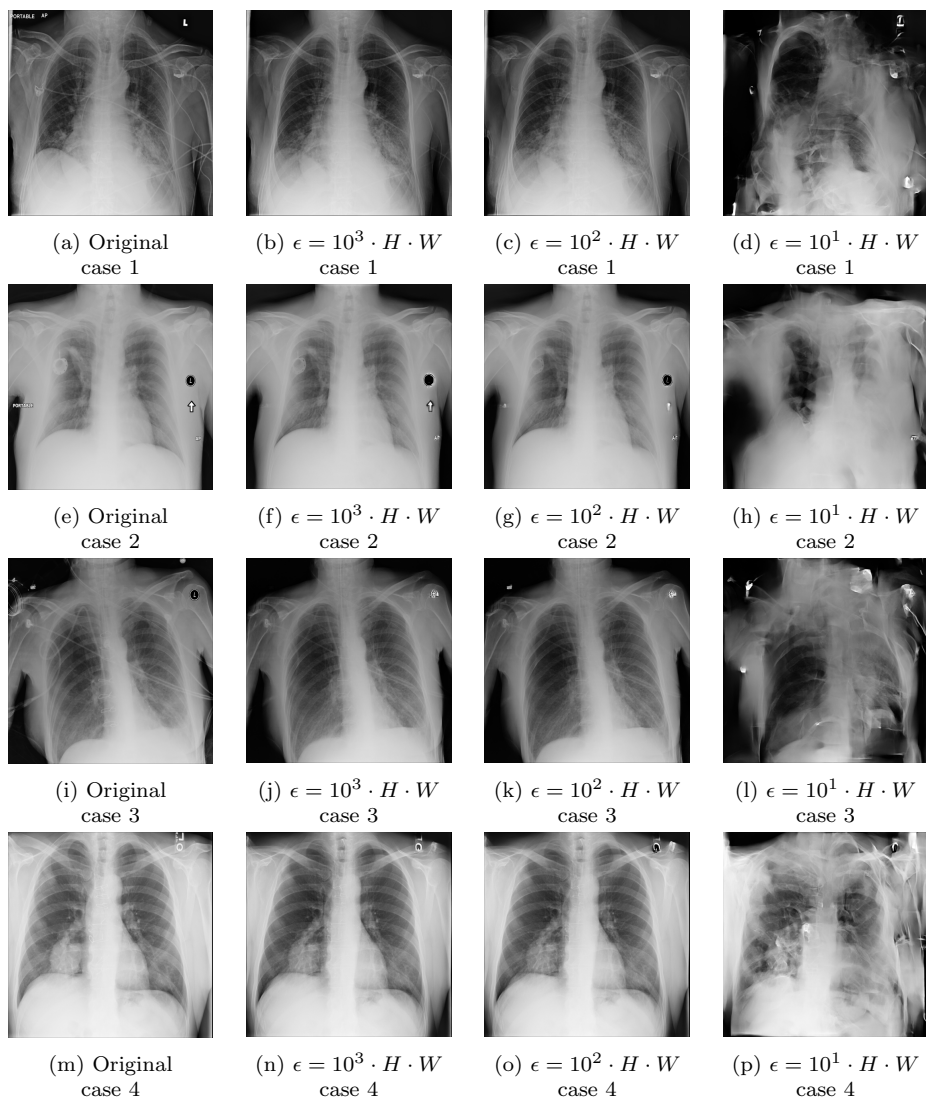
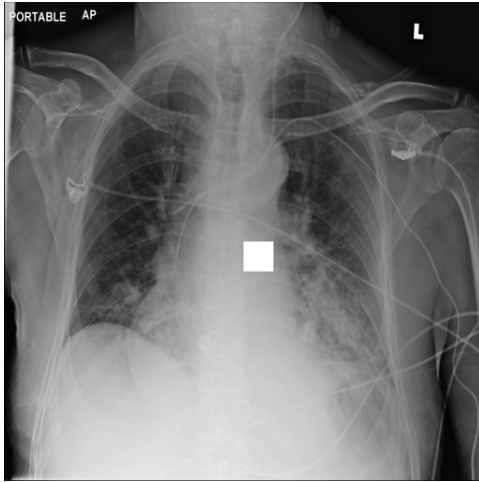
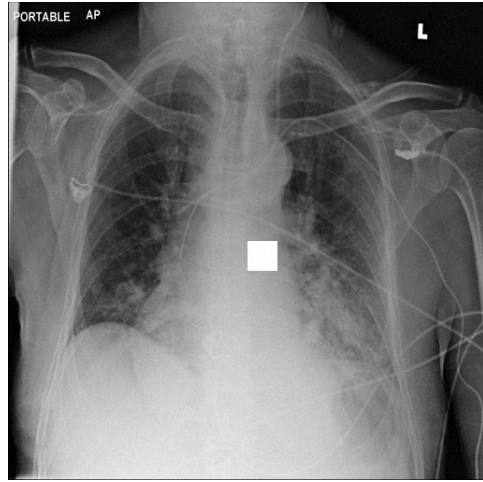


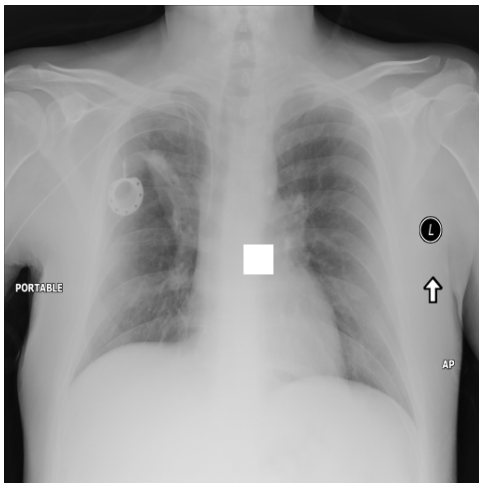
Figure 2: ϵ -LDP-processed CXR images obtained with DP-GLOW.



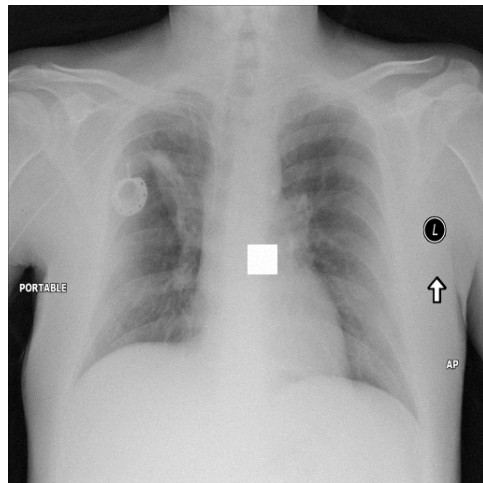
(a) Original,
case 1 with a block.



(b) $\epsilon = 10^2 \cdot H \cdot W$,
case 1.

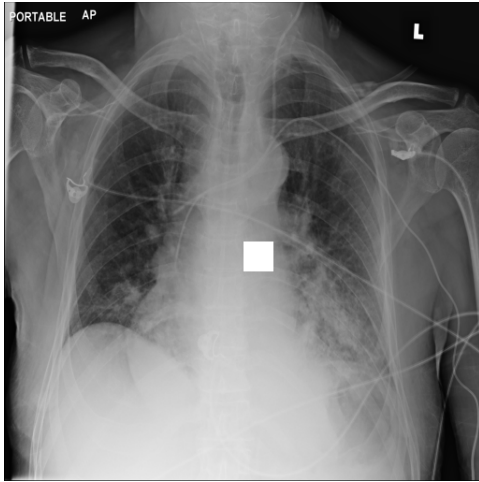


(c) Original,
case 2 with a block.



(d) $\epsilon = 10^2 \cdot H \cdot W$,
case 2.

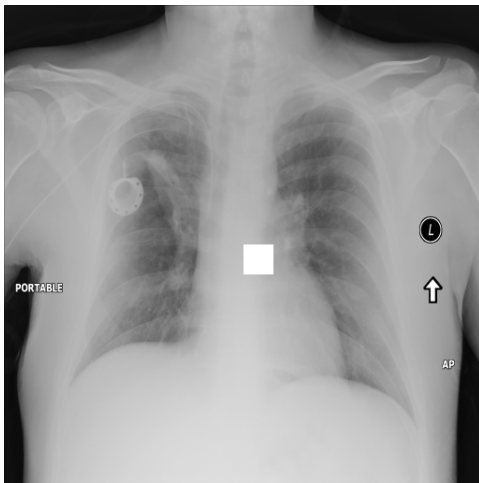
Figure 3: Block obfuscation with the image domain LDP.



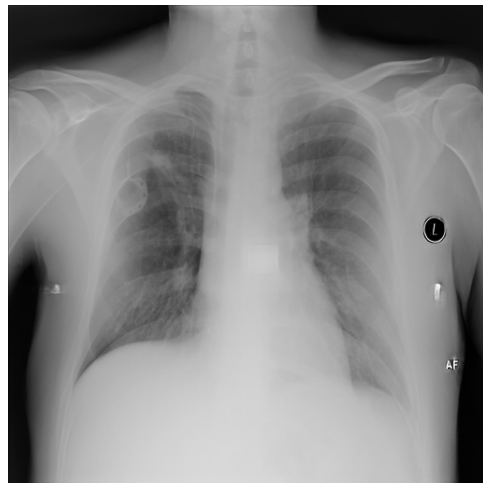
(a) Original,
case 1 with a block.



(b) $\epsilon = 10^2 \cdot H \cdot W$,
case 1.

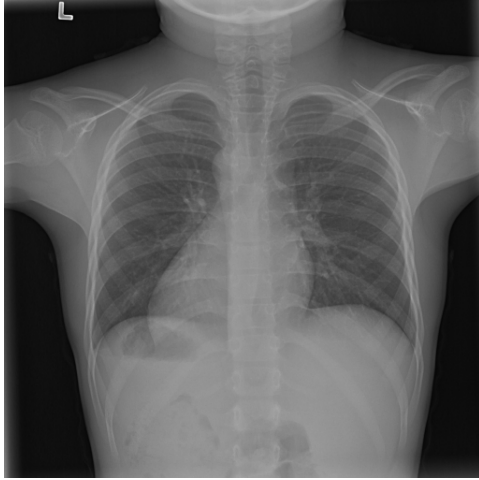


(c) Original,
case 2 with a block.

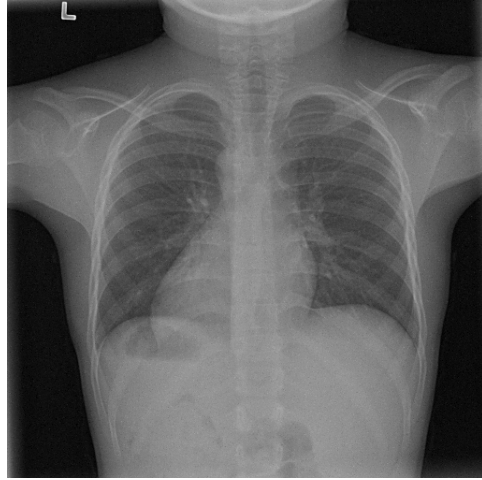


(d) $\epsilon = 10^2 \cdot H \cdot W$,
case 2.

Figure 4: Block obfuscation with DP-GLOW.

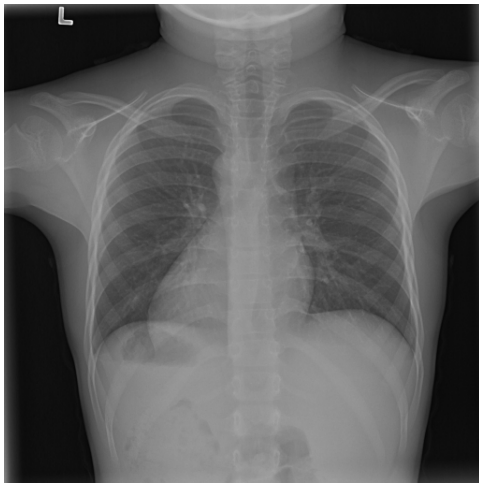


(a) Original,
case 5 (simulated *situs inversus*).

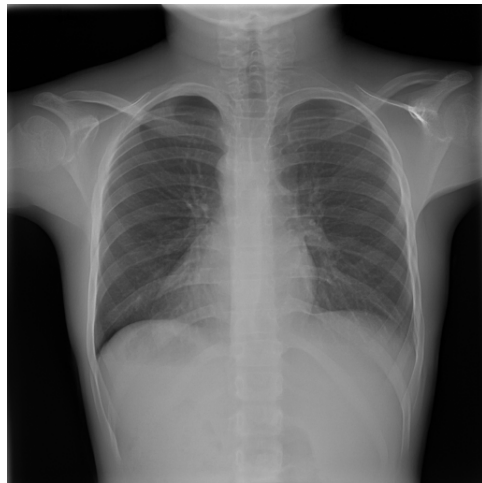


(b) $\epsilon = 10^2 \cdot H \cdot W$,
case 5.

Figure 5: Flip obfuscation with the image domain LDP.



(a) Original,
case 5 (simulated *situs inversus*).



(b) $\epsilon = 10^2 \cdot H \cdot W$,
case 5.

Figure 6: Flip obfuscation with DP-GLOW.